SIN-CHN SCIENTIFIC PRESS PTE.LTD.

Molecular & Cellular Biomechanics 2025, 22(3), 1348.
https://doi.org/10.62617/mcb1348

Article

Research on the antistatic performance of peanut shells @ glucose biochar/epoxy composites

Mengxiao Guo, Heyi Ge*, Boming Zhang, Jinman Liu

School of Materials Science and Engineering, University of Jinan, Jinan 250022, China
*** Corresponding author:** Heyi Ge, mse_gehy@ujn.edu.cn

CITATION

Guo M, Ge H, Zhang B, Liu J. Research on the antistatic performance of peanut shells @ glucose biochar/epoxy composites. Molecular & Cellular Biomechanics. 2025; 22(3): 1348. https://doi.org/10.62617/mcb1348

ARTICLE INFO

Received: 14 January 2025
Accepted: 10 February 2025
Available online: 18 February 2025

Abstract: In this work, the glucose nanocarbon spheres (GC) were in situ decorated on the surface of lamellar peanut shell biochar (PSAC) to construct the self-modified conductive function unit of biomass (PSAC@GC). The effects of PSAC@GC at different carbonization temperatures on the conductivity, the antistatic properties, and the thermal stability of epoxy composites were investigated. This unique structure not only improves the dispersion of GC nanospheres in the epoxy resin, but the larger carbon framework of PSAC also contributed to forming a continuous conductive network. Moreover, the well-dispersed GC nanospheres on PSAC facilitate the transfer of surface free electrons, effectively improving the electrical conductivity and ultimately strengthening the antistatic properties of the composites. The results show that when the carbonization temperature was 900 ℃, the conductivity of PSAC@GC with a mass ratio of 1:1 was 41.19 S/m, which represents an increase of 135% and 43% compared to PSAC and GC, respectively. When 5 wt.% PSAC@GC was added, it showed good dispersion in the epoxy resin, and the surface resistivity of the composites was reduced to 1.89 × 108 Ω. The work provides a new approach for the development of environmentally friendly and cost-effective novel antistatic carbon material.

Keywords: biochar; in-situ modification; antistatic performance; biochar epoxy composites

1. Introduction

In areas such as electronics and electrical appliances, as well as in our daily lives, the insulating materials are prone to the accumulation of static electricity, which can lead to equipment failure and even serious explosion incidents [1]. Moreover, in the packaging industry, particularly in the packaging of food, pharmaceuticals, and cosmetics, electrostatic accumulation may lead to the tearing or damage of packaging materials, thereby compromising the integrity of the packaging and the quality of the product [2]. Therefore, it is necessary to implement appropriate static electricity elimination for insulating materials to prevent potential problems. As a result, anti-static composites have emerged that can quickly conduct electricity, eliminate static and reduce the surface resistivity of insulating materials. The production of antistatic composites has become the focus of research [3,4].

The traditional method of reducing the resistivity of insulating polymers is to add conductive fillers, also called antistatic agents. The most commonly used conductive fillers currently include metal-based fillers, carbon-based fillers, and conductive polymer fillers, among others. Among them, carbon-based fillers are preferred by researchers for their ability to improve the electrical conductivity and thermal stability of polymers [5–7]. There are many reports on the addition of carbon materials in composites, including carbon black (CB) [8], graphene [9], carbon nanotubes (CNTs)

[10], and glassy carbon [11,12]. Although these materials have significant antistatic effects, their complex manufacturing processes and high costs are the main factors hindering the widespread use of carbon-based filled in industrial production. Due to concerns about economic costs and resource sustainability, some researchers have pyrolyzed waste biomass from daily life at high temperatures, forming a graphene-like structure to replace expensive carbon-based fillers [13]. Renewable and sustainable biochar has been increasingly applied in recent years as a conductive material in fields such as capacitor electrode materials and bioelectrochemical sensors [14,15]. It is emphasized that the electrical conductivity of biochar plays a crucial role in enhancing the capacitance and sensitivity of composite materials. However, some studies have shown that certain biomass-derived materials, after carbonization or modification, can effectively enhance their electrical conductivity, making them suitable for electrostatic discharge applications. Giorcelli et al. [16] used miscanthus as a carbon source, achieving a maximum electrical conductivity of 2.75 S/m for the biochar produced. Giorcelli et al. [17] used coffee waste as a carbon source and the carbonized coffee biochar reached a maximum electrical conductivity of 35.96 S/m, the conductivity of the biomass composite with the additional amount of 15wt% reached 1.85×10^{8} Ω. Poulose et al. [18] used palm as a carbon source, as the biochar content increased to 15 wt.%, the electrical conductivity of the composite improved by four orders of magnitude.

As an agricultural by-product, peanut shells are produced in large quantities every year, but their availability is very limited [19,20]. However, the high-temperature carbonized peanut shells (PSAC) have a layered structure similar to that of graphene [21]. The experiments have shown that PSAC can be used as a conductive filler to improve electrical conductivity, but most studies have focused primarily on the electrochemical and adsorption field, with relatively little research on polymer antistatic [22,23]. The glucose can also form spherical graphene structures (GC) over a wide temperature range of 500 to 800 ℃ [24]. And its high electrical conductivity has attracted wide attention. However, the severe agglomeration of carbon nanoparticles limits their application [25]. Many researchers have solved the agglomeration problem of nanospheres by using surfactants or organic dispersants [26–28]. However, these methods are relatively complex, and research on the antistatic properties of nanospheres is still limited.

In this work, the self-modified conductive function unit of biomass PSAC@GC was successfully produced by in-situ modification. A series of characterization methods including X-ray diffraction (XRD), Fourier transform infrared spectroscopy (FT-IR), and scanning electron microscopy (SEM) confirmed that GC nanospheres were successfully carbonized on the surface of PSAC and showed good dispersion. A detailed study was carried out on the electrical conductivity of PSAC@GC and the antistatic properties of its composites. PSAC@GC not only improved the dispersion of GC nanospheres in the epoxy resin, but the larger carbon framework of PSAC also contributed to forming a continuous conductive network. Moreover, the well-dispersed GC nanospheres on PSAC facilitated the transfer of surface free electrons, effectively increasing the electrical conductivity and ultimately improving the antistatic properties of the composites. Therefore, environmentally friendly and low-

cost biochar fillers are expected to replace expensive carbon-based materials and serve as a new type of antistatic agent.

2. Experimental

2.1. Materials

Peanut shells were collected from rural areas in Jinan, China. D-(+)-glucose was purchased from Shanghai Aladdin Biochemical Technology Co., Ltd. bought. Epoxy resin E-51 and hardener 593 were from Guangzhou Suixin Chemical Co., Ltd. bought. All chemical reagents (absolute ethanol, sodium hydroxide, hydrochloric acid) are of analytical quality (AR). Deionized water was prepared by our laboratory.

2.2. Preparation of PSAC@GC

The peanut shells were washed repeatedly with deionized water to remove surface contaminants and dust. They were ground into powder by a wall-breaking mill and then sieved through a 100-mesh sieve. The D-(+)-glucose was subjected to a hydrothermal carbonization treatment: [29] 5 g of glucose was completely dissolved in 50 mL of deionized water, and placed in a high-pressure reactor at 190 ℃ for 5 h. The hydrothermal glucose solution was centrifuged at 8000 rpm for 15 min. The precipitate was then washed repeatedly with deionized water and absolute ethanol until the filtrate became clear. Then it is dried at 70 ℃ and ground into powder.

Equal amounts of peanut shell powder and hydrothermal glucose powder were added respectively to the 0.1 M NaOH solution and magnetically stirred for 3 h. The mixtures were then placed in an oven at 70 ℃ for 12 h for incubation. After the pH was adjusted to 7 with HCl solution, the mixtures were washed repeatedly by suction filtration with deionized water and absolute ethanol. After drying again, producing two types of activated biomass powders. They were mixed in 1:2, 1:1 and 2:1 mass ratio and repeatedly ground until completely mixed. The mixed powders were carbonized under a nitrogen atmosphere with a heating rate of 5 ℃/min and held at 700 ℃, 800 ℃ and 900 ℃ for 2 h to obtain the PSAC@GC. The preparation process is shown in **Figure 1**. For convenience, the three biochar samples of different mass ratios were referred to as PSAC@GC-1, PSAC@GC-2, and PSAC@GC-3 respectively. At the same time, individual biochar samples were carbonized under the same conditions to obtain the PSAC and GC. The abbreviations of the biochar sample names are listed in **Table 1**.

Table 1. Abbreviations for the biochar samples.

Samples	Ratio (PSAC: GC)	Temperature/℃	Time/h
PSAC	——	700 800 900	2
GC	——	700 800 900	2
PSAC@GC-1	1:2	700 800 900	2
PSAC@GC-2	1:1	700 800 900	2
PSAC@GC-3	2:1	700 800 900	2

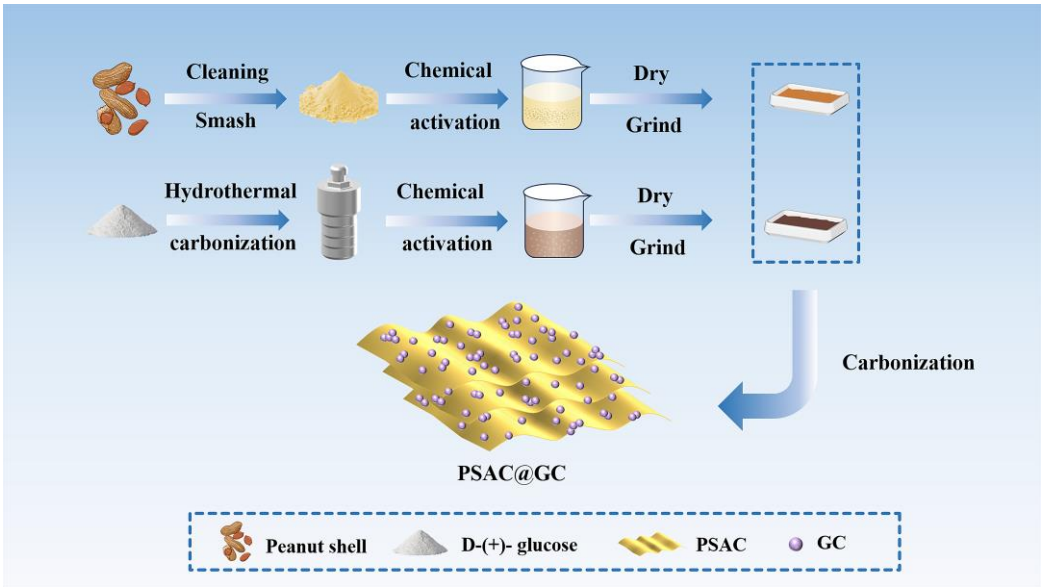

Figure 1. Flowchart of the preparation process of PSAC@GC.

2.3. Preparation of PSAC@GC epoxy composites

The 5, 10, 15, and 20 wt.% of PSAC@GC (a mass ratio of 1:1) were added to the epoxy resin. After stirring thoroughly, they were sonicated for 3 min and then a vacuum was applied for 30 min to remove any bubbles. Finally, the mixtures were poured into silicone molds with a diameter of 10 mm and a thickness of 2 mm after adding the curing agent. After curing at room temperature for 24 h and heating at 80 ℃ for 2 h, the samples were removed from the mold, producing the biochar composites. For systematic comparison, the epoxy resin without the addition of biochar was used as a blank sample and was called Pure epoxy. The above steps were repeated to obtain the individual biochar composites and the physically mixed biochar composites (a mass ratio of 1:1). The abbreviations of the biochar composites sample names are listed in **Table 2**.

Table 2. Abbreviations for biochar composite samples.

Samples	Biochar	Filler content (wt.%)
Pure epoxy	No biochar	0 wt.%
PSAC/EP	PSAC	5, 10, 15, 20 wt.%
GC/EP	GC	5, 10, 15, 20 wt.%
PSAC@GC/EP	PSAC@GC (mass ratio 1:1)	5, 10, 15, 20 wt.%
PSAC-GC/EP	PSAC-GC (Physical mixing, mass ratio 1:1)	5, 10, 15, 20 wt.%

2.4. Characterization

A Bruker D8 ADVANCE diffractometer applied an X-ray diffraction (XRD) test to identify the crystal structure of the samples. Fourier transform infrared spectroscopy (FTIR, Nicolet 380) was used to examine surface functional groups. A scanning electron microscope (SEM, QUANTA 250 FEG) was used to analyze the microstructure and dispersion of the samples. A Netzsch TG 209 F3 Tarsus thermal gravimetric analyzer from Germany was used to analyze the thermal weight loss

behavior of the samples. The RIGOL DM3068 digital multimeter was used to test the electrical conductivity of the biomass carbon. Each group of the samples was tested at five points in different locations, and the average value was taken. Calculate the conductivity of the sample using the following relationship:

$$\sigma = \frac{L}{R \cdot A}$$

In the formula, R represents the powder resistivity value (Ω), σ represents the powder conductivity (S/m), A represents the surface area of each electrode (m^2), and L represents the distance between the two copper electrodes (m).

The GEST-121A automatic insulation resistivity tester from Beijing Guance Precision Instrument Co., Ltd. was used to test the surface resistivity of the epoxy resin composites according to the GB/T 31838.3-2019. The voltage was set to 100 V. Each group of the test samples was repeated three times, and the surface resistivity was averaged.

3. Results and discussion

3.1. XRD

Figure 2 shows the XRD patterns of PSAC, GC, and PSAC@GC(mass ratio 1:1) under the carbonization condition of 900 ℃ for 2 h. Firstly, a broad peak for PSAC and GC is observed between 20° and 30°, and a weaker peak appears between 40° and 45°, corresponding to the (002) and (101) crystal planes of graphitic carbon, respectively [30]. This indicates that PSAC and GC both have a graphite-carbon structure. Furthermore, the low intensity and large width of the two diffraction peaks indicate that the biomass formed amorphous carbon characterized by ordered graphitic carbon fragments through high-temperature carbonization [31].

The XRD curve of PSAC@GC also shows similar peaks, indicating successful bond formation between PSAC and GC. However, compared to PSAC and GC, the diffraction peaks of PSAC@GC have higher intensity, indicating that PSAC@GC has developed a more pronounced graphite-carbon structure.

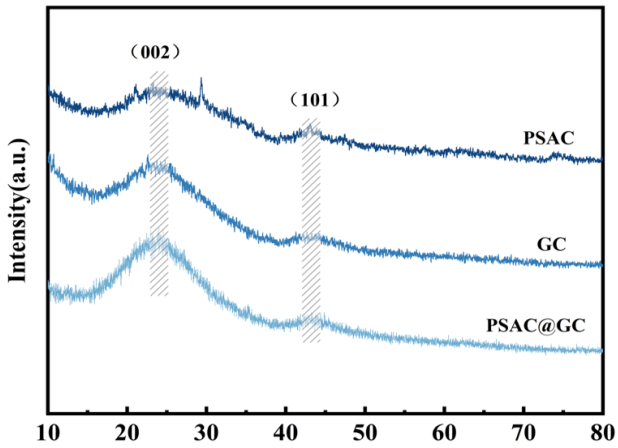

Figure 2. The XRD patterns of PSAC, GC, and PSAC@GC.

3.2. FT-IR

Figure 3 shows the FT-IR spectra of PSAC, GC, and PSAC@GC (mass ratio 1:1) under the carbonization condition of 900 ℃ for 2 h. They all exhibit three different absorption peaks at 3437 cm^{-1}, 1630 cm^{-1}, and 922 cm^{-1}, which are attributed to the stretching vibrations of –OH, C = C, and C–O–C bonds, respectively [32]. In conjunction with the XRD data analysis, it is observed that the biochar has formed a graphene-like structure after the high-temperature pyrolysis and the oxygen-containing functional groups are present.

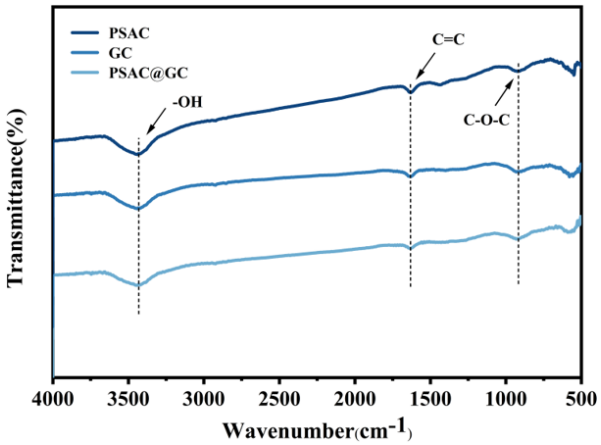

Figure 3. The FT-IR spectra of PSAC, GC and PSAC@GC.

3.3. The microstructure

3.3.1. Biochar

The SEM images are shown in **Figure 4**. There are significant morphological differences between PSAC and GC. Looking at **Figure 4a–c**, it can be seen that PSAC has a three-dimensional layered structure with stacked layers that have pronounced texture and roughness. Looking at **Figure 4d–f**, the GC nanospheres are present in the form of interconnected nanospheres. As shown in **Figure 4f**, the size is approximately between 200 nm and 500 nm. The three-dimensional layer structure of PSAC as well as the cross-linked carbon nanospheres structure of GC gives the biochar a high specific surface area. This implies that a larger number of free electrons can participate in the conduction process [33–35].

Figure 4g–i show the micromorphology of PSAC@GC, where a significant amount of GC nanospheres can adhere to the surface of the PSAC layers, indicating that the GC nanospheres on PSAC have occurred successfully. At the same time, the GC nanospheres are not only distributed on the surface of the PSAC, but are also observed to adhere in the interlayer spaces. The successful attachment of GC on the PSAC surface is a complex process that involves a combination of different interactive effects. Firstly, they both are made of carbon elements, and the van der Waals forces act between them. The interaction of instantaneous dipole moments between nonpolar molecules contributes to the initial adhesion of GC on the surface of PSAC [36]. In addition, glucose molecules undergo dehydrogenation, condensation and carbonization during the hydrothermal carbonization process [26], resulting in colloidal spheres rich in functional groups [37]. The hydroxyl and carboxyl groups on

the surface of the nanospheres can form hydrogen bonds or more stable chemical bonds with the oxygen-containing functional groups on the surface of PSAC, thereby improving adhesion [38–40]. In addition, the porous structure and rough surface of PSAC increase friction and contact points, making GC easier to adhere to the surface. This structure helps alleviate the serious agglomeration problem of GC. Meanwhile, the successful carbonization of GC on the PSAC surface facilitates the transfer of free electrons on the surface, resulting in stronger electric current conduction.

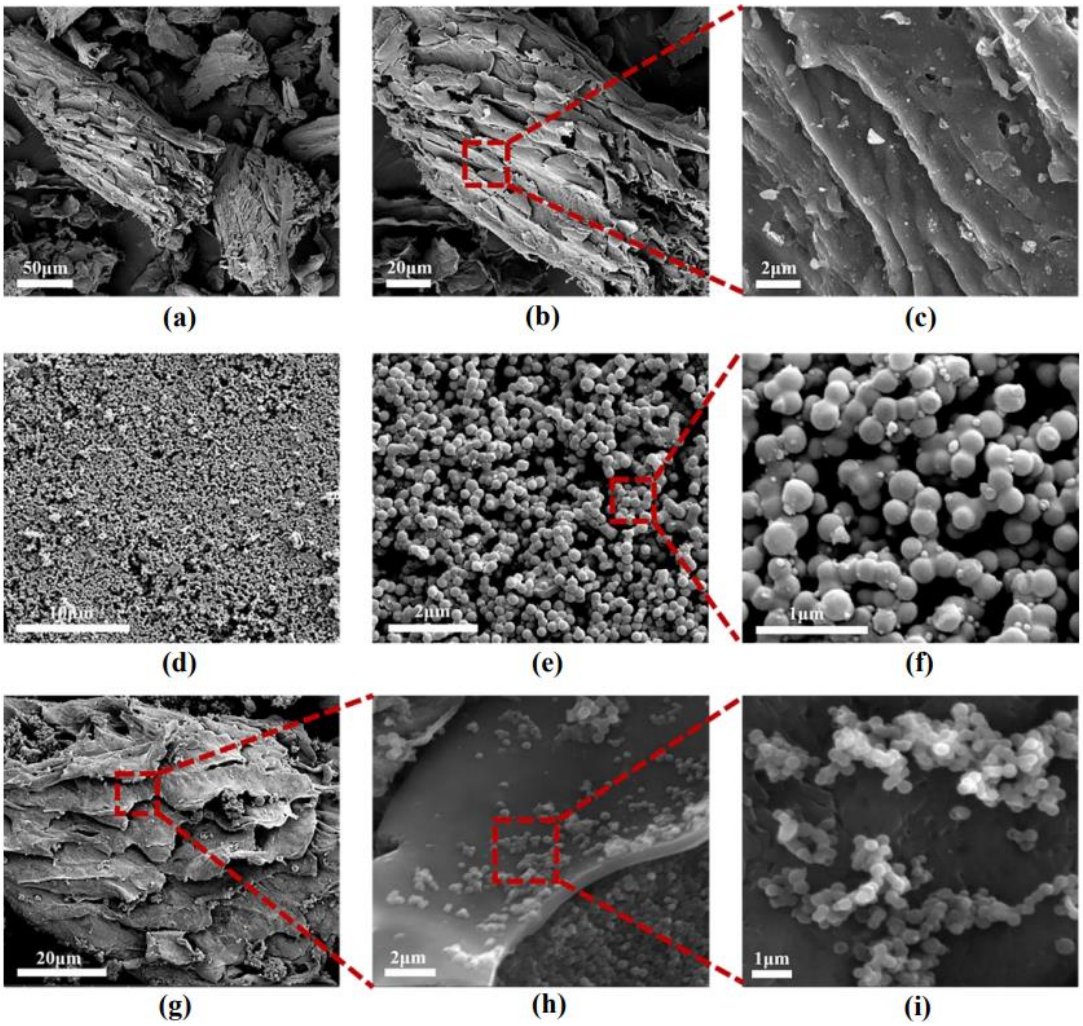

Figure 4. The SEM images of PSAC, GC and PSAC@GC: **(a–c)** PSAC; **(d–f)** GC; **(g–i)** PSAC@GC.

3.3.2. Biochar composites

Figure 5 shows the morphological characterization of the fracture surfaces of 5 wt.% GC/EP and 5 wt.% PSAC@GC/EP after a low-temperature fracture. In **Figure 5a–c**, the large GC agglomerate within the GC/EP can be observed. Looking at **Figure 5c**, the red arrows point to the boundary between the GC nanospheres and the epoxy resin, indicating that the GC nanospheres are completely encapsulated by the epoxy resin, forming discrete "island-like" structures that have no connection to other GC clusters. This demonstrates the inherent poor dispersibility of GC, which leads to severe agglomeration within the epoxy resin. In **Figure 5d**, the red circles show the distribution of PSAC@GC in the epoxy resin, while the red arrows indicate the GC

nanospheres that were not successfully adherent. Compared to GC/EP, the PSAC@GC is more evenly distributed in the epoxy resin. Although agglomerate GC nanospheres are still present, they no longer form concentrated agglomerations, instead are distributed into smaller, scattered pieces, forming a more coherent dispersion system with PSAC@GC.

Looking further at **Figure 5e–f**, the yellow arrows indicate the independently distributed GC. It can be observed that the GC attached to the surface of PSAC is no longer agglomerated but exists as independent carbon spheres. Even if the GC nanospheres separate from the PSAC surface due to weaker adhesion, they can still be well distributed in the epoxy resin matrix. The SEM images show that PSAC@GC has better dispersion in the epoxy resin compared to GC, which favors the formation of a continuous conductive network.

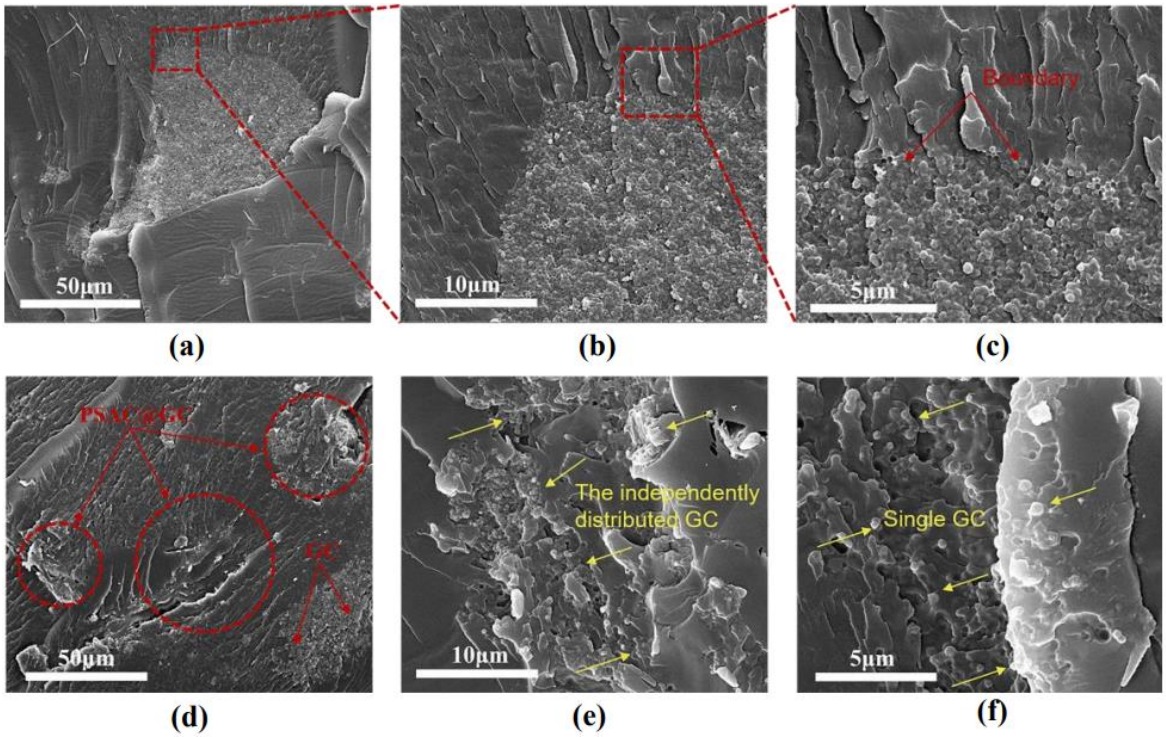

Figure 5. SEM images of composites with 5 wt.% loading: **(a–c)** GC/EP; **(d–f)** PSAC@GC/EP. (Magnifications at ×1000, ×5000 and ×10000).

3.4. Electrical conductivity of biochar

The trend of conductivity as a function of temperature is shown in **Figure 6a**. It can be observed that the conductivity of the biochar significantly increases with rising temperature. This is mainly due to the crystalline structure of carbon gradually improving, and the bonding between carbon atoms becomes more stable, while the degree of graphitization of carbon also increases at higher temperatures. Additionally, high temperatures help remove volatile components, reduce the content of other elements (such as oxygen, nitrogen, and hydrogen) in the biomass, and increase the overall carbon content, thereby improving conductivity [41,42].

The electrical conductivity of different biochar is analyzed under carbonization conditions of 900 ℃ for 2 h (**Figure 6b**). The PSAC exhibits relatively weak

conductivity. This is mainly due to the insufficient surface graphitization of PSAC after high-temperature carbonization, which limits its ability to exhibit high electrical conductivity. In contrast, the electrical conductivity of GC is significantly higher than that of PSAC at 28.88 S/m. This is mainly attributed to the effective removal of impurities and volatiles during hydrothermal carbonization of GC, resulting in a denser carbon structure. This increased density facilitates a more ordered arrangement of carbon atoms during the subsequent high-temperature carbonization process, thereby promoting graphitization [43]. After performing in situ modification of PSAC and GC at different ratios, the electrical conductivity also changed. Specifically, at a mass ratio of 1:1, the conductivity reached 41.19 S/m, which represents an increase of 135% and 43% compared to PSAC and GC, respectively. This is mainly attributed to after the carbonization of GC on the surface of PSAC, the increased conductivity of GC exposes more electron transport sites [44,45], which facilitates electron transitions and forms a more efficient conductive network [46,47]. The PSAC@GC structure facilitates the formation of a continuous conductive network while improving internal current conduction, thereby achieving improved electrical conductivity.

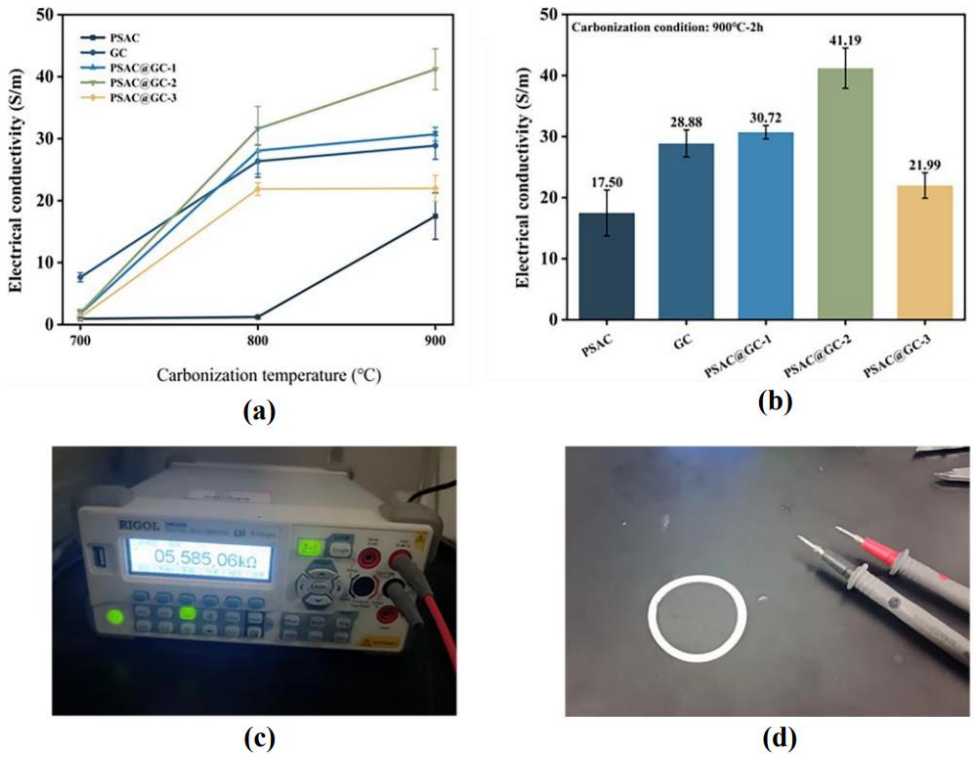

Figure 6. (a) Electrical conductivities of different temperature; **(b)** electrical conductivities of different biochar (900 ℃-2h); **(c)** the RIGOL DM3068 digital multimeter; **(d)** biochar test sample.

3.5. Antistatic performance of composites

Based on the comparison of the electrical conductivity of biochar, we select PSAC@GC-2 with a mass ratio of 1:1 as the conductive filler for further experiments (hereafter referred to as PSAC@GC). This filler is respectively mixed with epoxy resin at loadings of 5 wt.%, 10 wt.%, 15 wt.%, and 20 wt.% to prepare the biochar epoxy composites. The antistatic performance is then compared by testing the surface

resistivity of the composites. The biochar composite samples and instruments are shown in **Figure 7**.

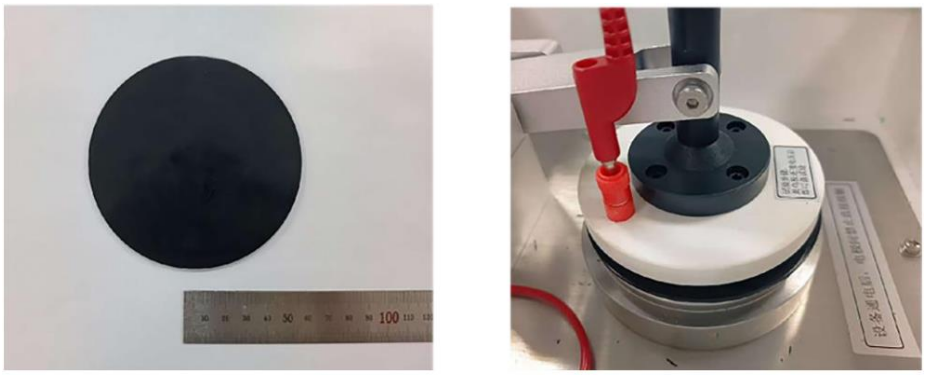

(a) **(b)**

Figure 7. (a) The sample of biochar composite material; **(b)** The automatic insulation resistivity tester.

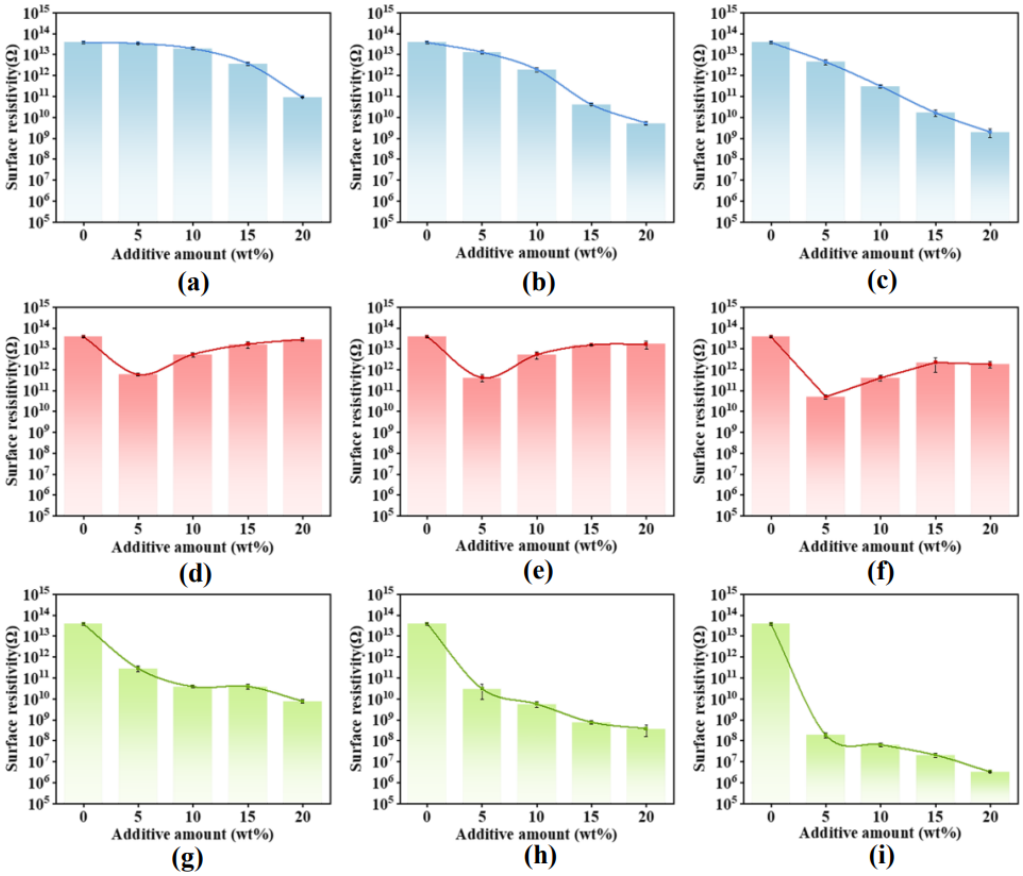

Figure 8. The change of surface resistivity of biochar composites with addition amount: **(a–c)** PSAC/EP (700, 800, 900 ℃); **(d–f)** GC/EP (700, 800, 900 ℃); **(g–i)** PSAC@GC/EP (700, 800, 900 ℃).

As shown in **Figure 8**, as the amount of biochar increased, the surface resistivity of the epoxy composites changed. Due to the differences in electrical conductivity of biochar caused by carbonization temperature, the biochar obtained at 900 °C exhibits the most significant antistatic effect in the epoxy composites. The surface resistivity of PSAC/EP decreases relatively gradually and reaches 10^9 Ω when the additive content is 20 wt.%. The surface resistivity of PSAC@GC/EP decreases by five orders

of magnitude, reaching 10^8 Ω at a loading of 5 wt.%. After that, the decrease slows down, with a value of 10^6 Ω at 20 wt.%. This indicates that at 5 wt.%, the biochar has formed a continuous conductive network within the epoxy resin, and further increases in loading do not result in significant improvements. With GC/EP, at an additive content of 5 wt.%, there is a brief decrease in surface resistivity, but as the amounts of additive increases, the surface resistivity then increases again. This proves the tendency of GC to agglomerate easily, and as the loading increases, the agglomeration becomes more severe, resulting in progressively poorer antistatic performance.

According to the ANSI/ESD STM11.11-2011 standard, the surface resistivity of electrostatic dissipative materials is typically between 10^6 and 10^9 Ω. As shown in **Figure 8**, the PSAC@GC/EP achieves the antistatic requirements when the additive content is 5 wt.%. To provide a clearer analysis of the experimental results, we used an additive content of 5 wt.% as a reference point to systematically evaluate the antistatic performance of different composites. Looking at **Figure 9**, it is found that the surface resistivity of pure epoxy resin is 3.79×10^{13} Ω. The surface resistivity of PSAC/EP is observed to be 4.50×10^{12} Ω, which is a decrease of only one order of magnitude related to the low conductivity of PSAC. The surface resistivity of GC/EP is 5.05×10^{10} Ω, indicating that the antistatic performance is still poor, which is inconsistent with the relatively high conductivity of GC. This is mainly due to the GC leads to severe aggregation within the epoxy resin, as shown in **Figure 5a–c**. After adding the 5 wt.% physically mixed PSAC-GC, the surface resistivity decreases to 1.71×10^{10} Ω. This still does not achieve the desired effect. The surface resistivity of PSAC@GC/EP with 5 wt.% additive is 1.89×10^8 Ω, which meets the antistatic standards for composites. This indicates that the PSAC@GC achieved uniform distribution within the epoxy resin, forming a more continuous and efficient conductive network. **Table 3** summarizes the results obtained by other researchers on the antistatic properties of carbon-based composites.

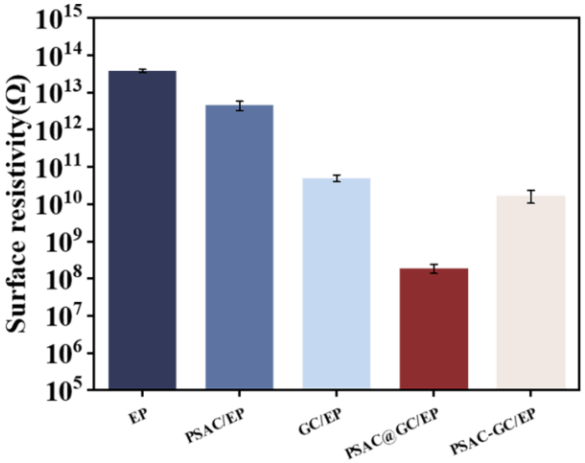

Figure 9. The surface resistivity at 5wt%.

Table 3. The antistatic properties of carbon-based composites.

Samples	Matrix	Filler content (wt.%)	Surface resistivity(Ω)	Refs.
RGO	CS/gelatin	20 wt.%	9.87×10^{5}	[48]
CB	PP/PA6	10 wt.%	1.02×10^{6}	[49]
GNPs @PANI	EVA/HDPE	10 wt.%	3.20×10^{5}	[50]
MWCNTs	PS/PPO	4 wt.%	10^{6}	[51]
CNTs	PC/PBT	2 wt.%	1.50×10^{6}	[6]
Bamboo biochar	UHMWPELLDPE	80wt.%	9.29×10^{-3}	[52]
Powder biochar	UHMWPE	70wt.%	1.75×10^{-1}	[53]
Coffee biochar	EP	15wt.%	1.85×10^{6}	[17]
PSAC@GC	**EP**	**5 wt.%**	**1.89×10^{8}**	**This work**

3.6. Thermal stability analysis

Figure 10 shows the mass loss curves of pure epoxy resin and biochar composites containing 5 wt.% PSAC/EP, GC/EP, PSAC-GC/EP, and PSAC@GC/EP. The pure epoxy resin begins to decompose at around 340 ℃ and the thermal decomposition stabilizes at 500 ℃. This is mainly due to the breakdown of bonds, which leads to the decomposition of various phenolic compounds [54]. Except for PSAC/EP, which remains stable until the decomposition temperature is reached, other composites show a similar downward trend in stability. This is due to the higher content of decomposable carbon in the hydrothermally treated GC [55]. In addition, the decomposition temperature of biochar composites is higher and remains significant amounts of residues. The residue percentages are as follows: Pure epoxy residue is 16.45%, PSAC/EP is 20.55%, GC/EP is 17.64%, PSAC-GC/EP is 24.40% and PSAC@GC/EP is 25.05%. The incorporation of biochar materials also helps improve the thermal stability of epoxy resin. This is because biochar produced at higher temperatures typically has better thermal stability, which is related to the degree of aromatization of the carbon structure in the biochar. The PSAC@GC exhibits the highest thermal stability, which is not only due to its inherent high thermal stability, but also because it can form a heat absorption and dissipation network within the composite material, thereby improving the heat resistivity of the epoxy polymer. This further shows the good dispersibility of PSAC@GC in the epoxy resin. The TGA data is shown in **Table 4**.

Table 4. TGA data of composites with 5 wt.% loading.

Composites samples	$T_{10\%}$ (℃)	T_{MAX} (℃)	Weight at 500 ℃ (wt.%)
Pure epoxy	313	356	16.45
PSAC/EP	334	359	20.55
GC/EP	329	361	17.64
PSAC-GC/EP	324	366	24.40
PSAC@GC/EP	329	359	25.05

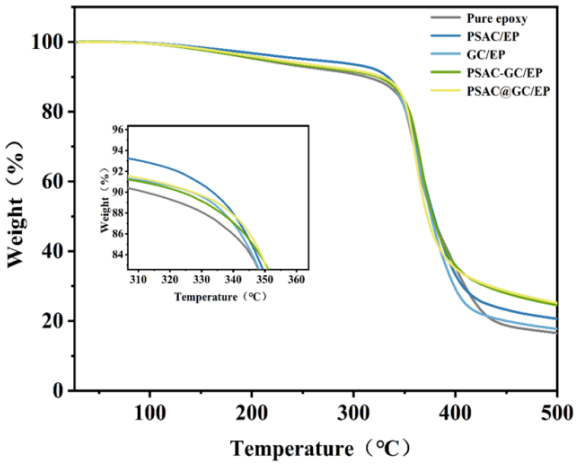

Figure 10. TGA of composites with 5 wt.% loading.

3.7. Antistatic mechanism

Figure 11 illustrates the antistatic mechanisms present in GC/EP and PSAC@GC/EP. It is generally believed that there are two conduction principles: the tunnel effect theory and the conductive path theory [56,57]. **Figure 11a** illustrates the antistatic mechanism of GC in epoxy resin. It can be seen that GC is highly agglomerated and the GC clusters GC clusters are far away from each other, resulting in free electrons not being able to move through the tunneling effect.

Figure 11b illustrates the antistatic mechanism of PSAC@GC in epoxy resin. The uniform distribution of GC on the surface of PSAC improves agglomeration. Furthermore, the larger carbon framework of PSAC and the agglomeration of the unloaded small GC fragments increase the contact area of the conductive fillers. This leads to tunneling effects between the conductive fillers, allowing electrons to move freely through the tunneling effect between the carbon fillers, forming a conductive network throughout the epoxy resin. In addition, after the successful carbonization of GC on the surface of PSAC, the highly conductive GC nanospheres increase the electron transport sites, which facilitates the transfer of free electrons and leads to stronger current conduction within the conductive network, thereby improving the antistatic properties of the epoxy resin.

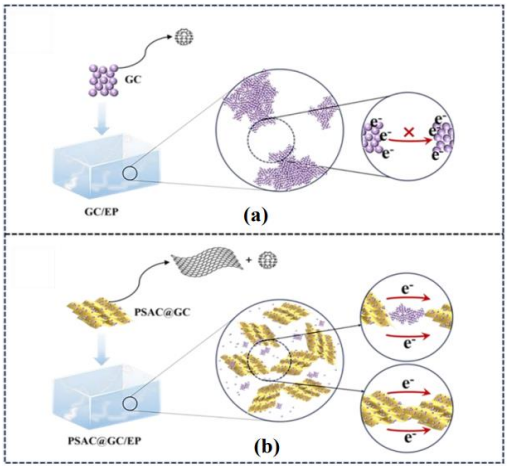

Figure 11. Antistatic mechanisms of biochar epoxy composites: **(a)** GC/EP; **(b)** PSAC@GC.

4. Conclusions

In sum, the self-modified conductive function of biochar PSAC@GC was successfully produced by simple in-situ modification. The results show that the PSAC@GC structure not only improves the agglomeration problem of GC but also forms a continuous and efficient conductive network. Moreover, the introduction of GC provides more electron transport sites and improves current conduction. When the mass ratio of PSAC to GC is 1:1, the conductivity of PSAC@GC obtained at 900 ℃ reaches 41.19 S/m. When 5 wt.% PSAC@GC is added, and the surface resistivity of the epoxy composite decreases to 1.89×10^8 Ω, meeting the antistatic standard. This provides new carbon-functional materials that are both environmentally friendly and economically feasible, promoting the large-scale application of biochar in industrial fields. Although PSAC@GC demonstrates excellent performance, future research should focus on adjusting the surface functionalization of PSAC@GC to further enhance the mechanical properties, corrosion resistance, and stability of the composite, thereby enabling its broader industrial applications.

Author contributions: Methodology, MG; data curation, MG; writing—original draft preparation, MG; conceptualization, HG; writing—review and editing, HG; visualization, BZ; supervision, BZ; formal analysis and investigation, JL. All authors have read and agreed to the published version of the manuscript.

Funding: This work was supported by the Natural Science Foundation of Shandong, China [Grant No. ZR2020ME040].

Ethical approval: Not applicable.

Data availability statement: The data that support the findings of this study are available on request from the corresponding author.

Conflict of interest: The authors declare no conflict of interest.

References

1. Ge C, Devar G. Formation of Polyvinyl Alcohol film with graphene nanoplatelets and carbon black for electrostatic discharge protective packaging. Journal of Electrostatics. 2017; 89: 52–57. doi: 10.1016/j.elstat.2017.07.004
2. de Souza Vieira L, dos Anjos EGR, Verginio GEA, et al. Carbon-based materials as antistatic agents for the production of antistatic packaging: a review. Journal of Materials Science: Materials in Electronics. 2021; 32(4): 3929–3947. doi: 10.1007/s10854-020-05178-6
3. Gill YQ, Ehsan H, Irfan MS, et al. Synergistic augmentation of polypropylene composites by hybrid morphology polyaniline particles for antistatic packaging applications. Materials Research Express. 2020; 7(1): 015331. doi: 10.1088/2053-1591/ab61b5
4. Rafique I, Kausar A, Anwar Z, et al. Exploration of Epoxy Resins, Hardening Systems, and Epoxy/Carbon Nanotube Composite Designed for High Performance Materials: A Review. Polymer-Plastics Technology and Engineering. 2015; 55(3): 312–333. doi: 10.1080/03602559.2015.1070874
5. Dahal RK, Acharya B, Dony B, et al. Biocarbon Filled Hemp-Epoxy Composite: Its Physical, Mechanical, and Thermal Properties. Applied Composite Materials. 2022; 29(6): 2185–2202. doi: 10.1007/s10443-022-10059-8
6. Huang T, Li JL, Yang JH, et al. Carbon nanotubes induced microstructure and property changes of polycarbonate/poly(butylene terephthalate) blend. Composites Part B: Engineering. 2018; 133: 177–184. doi: 10.1016/j.compositesb.2017.09.037

7. He Y, Ju S, Duan K, et al. Tuning the through-thickness orientation of 1D nanocarbons to enhance the electrical conductivity and ILSS of hierarchical CFRP composites. Science and Engineering of Composite Materials. 2021; 28(1): 453–465. doi: 10.1515/secm-2021-0040
8. Xue P, Chen Z, Wei L, et al. PTFE-based antistatic coatings by incorporating modified carbon black. Nanotechnology. 2024; 36(2): 025702. doi: 10.1088/1361-6528/ad84fd
9. Hu H, Zhao J, Jiang D, et al. Preparation and PTC properties of multilayer graphene/CB/HDPE conductive composites with different cross-linking systems. Materials Science in Semiconductor Processing. 2024; 173: 108124. doi: 10.1016/j.mssp.2024.108124
10. da Silva FS, Luna CBB, da Silva Barbosa Ferreira E, et al. Polyamide 6 (PA6)/carbon nanotubes (MWCNT) nanocomposites for antistatic application: tailoring mechanical and electrical properties for electronic product protection. Journal of Polymer Research. 2024; 31(1). doi: 10.1007/s10965-023-03861-w
11. de Souza Vieira L, Montagna LS, Marini J, et al. Influence of particle size and glassy carbon content on the thermal, mechanical, and electrical properties ofPHBV/glassy carbon composites. Journal of Applied Polymer Science. 2020; 138(4). doi: 10.1002/app.49740
12. Oyama IC, de Souza GPM, Rezende MC, et al. A new eco-friendly green composite for antistatic packaging: Green low-density polyethylene/glassy carbon. Polymer Composites. 2020; 41(7): 2744–2752. doi: 10.1002/pc.25572
13. Tan X fei, Liu S bo, Liu Y guo, et al. Biochar as potential sustainable precursors for activated carbon production: Multiple applications in environmental protection and energy storage. Bioresource Technology. 2017; 227: 359–372. doi: 10.1016/j.biortech.2016.12.083
14. Liu L, Zhang W, Lu B, et al. Controllable heteroatoms doped electrodes engineered by biomass based carbon for advanced supercapacitors: A review. Biomass and Bioenergy. 2024; 186: 107265. doi: 10.1016/j.biombioe.2024.107265
15. Zhang H, Zhu W, Yang Z, et al. Highly conductive, mechanically robust and multi-purpose carbon aerogel composites derived from waste bread enable high-performance symmetric supercapacitors. Journal of Power Sources. 2024; 615: 235067. doi: 10.1016/j.jpowsour.2024.235067
16. Giorcelli M, Savi P, Khan A, et al. Analysis of biochar with different pyrolysis temperatures used as filler in epoxy resin composites. Biomass and Bioenergy. 2019; 122: 466–471. doi: 10.1016/j.biombioe.2019.01.007
17. Giorcelli M, Bartoli M. Development of Coffee Biochar Filler for the Production of Electrical Conductive Reinforced Plastic. Polymers. 2019; 11(12): 1916. doi: 10.3390/polym11121916
18. Poulose AM, Elnour AY, Anis A, et al. Date palm biochar-polymer composites: An investigation of electrical, mechanical, thermal and rheological characteristics. Science of The Total Environment. 2018; 619–620: 311–318. doi: 10.1016/j.scitotenv.2017.11.076
19. Sankaran S, Palani G, Yang YL, et al. Enhancing natural fiber-based polymeric composites with biochar filler particles derived from groundnut shell biomass waste. Biomass Conversion and Biorefinery. 2024; 1–12. doi: 10.1007/s13399-024-06201-0
20. Duan F, Zhang JP, Chyang CS, et al. Combustion of crushed and pelletized peanut shells in a pilot-scale fluidized-bed combustor with flue gas recirculation. Fuel Processing Technology. 2014; 128: 28–35. doi: 10.1016/j.fuproc.2014.06.022
21. Saravanan BA, Jayabalakrishnan D, Sambath S, et al. Influence of peanut husk waste–derived SiC particle on dry sliding wear, thermal, and electrical conductivity behaviors of abaca-vinyl ester composite. Biomass Conversion and Biorefinery. 2023; 15(1): 133–140. doi: 10.1007/s13399-023-04932-0
22. Pandey L, Sarkar S, Arya A, et al. Fabrication of activated carbon electrodes derived from peanut shell for high-performance supercapacitors. Biomass Conversion and Biorefinery. 2021; 13(8): 6737–6746. doi: 10.1007/s13399-021-01701-9
23. Zhan Y, Zhou H, Guo F, et al. Preparation of highly porous activated carbons from peanut shells as low-cost electrode materials for supercapacitors. Journal of Energy Storage. 2021; 34: 102180. doi: 10.1016/j.est.2020.102180
24. Liu X, Giordano C, Antonietti M. A Facile Molten-Salt Route to Graphene Synthesis. Small. 2013; 10(1): 193–200. doi: 10.1002/smll.201300812
25. Ischia G, Cutillo M, Guella G, et al. Hydrothermal carbonization of glucose: Secondary char properties, reaction pathways, and kinetics. Chemical Engineering Journal. 2022; 449: 137827. doi: 10.1016/j.cej.2022.137827
26. Liu S, Zhao Y, Zhang B, et al. Nano-micro carbon spheres anchored on porous carbon derived from dual-biomass as high rate performance supercapacitor electrodes. Journal of Power Sources. 2018; 381: 116–126. doi: 10.1016/j.jpowsour.2018.02.014

27. Xie H, Chong J, Tian Y, et al. A facile and environmentally friendly biomass-assisted stöber method to fabricate dispersed carbon nanospheres. Journal of Porous Materials. 2018; 26(1): 185–191. doi: 10.1007/s10934-018-0635-y
28. Singh JK, Rout AK. Thermal stability and dynamic mechanical analysis of nano-biofillers blended hybrid composites reinforced by cellulosic Borassus flabellifer L. fiber. International Journal of Polymer Analysis and Characterization. 2023; 28(6): 552–563. doi: 10.1080/1023666x.2023.2251792
29. Feng CN, Zhan XY, Li P, et al. Capacitive behavior of glucose-derived porous activated carbon with different morphologies. Journal of Alloys and Compounds. 2019; 805: 426–435. doi: 10.1016/j.jallcom.2019.07.093
30. Gong Y, Li D, Luo C, et al. Highly porous graphitic biomass carbon as advanced electrode materials for supercapacitors. Green Chemistry. 2017; 19(17): 4132–4140. doi: 10.1039/c7gc01681f
31. Wang D, Liu S, Fang G, et al. From Trash to Treasure: Direct Transformation of Onion Husks into Three-Dimensional Interconnected Porous Carbon Frameworks for High-Performance Supercapacitors in Organic Electrolyte. Electrochimica Acta. 2016; 216: 405–411. doi: 10.1016/j.electacta.2016.09.053
32. Zhang Y, Liu S, Zheng X, et al. Biomass Organs Control the Porosity of Their Pyrolyzed Carbon. Advanced Functional Materials. 2016; 27(3): 1604687. doi: 10.1002/adfm.201604687
33. Qi Y, Zhang M, Qi L, et al. Mechanism for the formation and growth of carbonaceous spheres from sucrose by hydrothermal carbonization. RSC Advances. 2016; 6(25): 20814–20823. doi: 10.1039/c5ra26725k
34. Zheng M, Liu Y, Xiao Y, et al. An Easy Catalyst-Free Hydrothermal Method to Prepare Monodisperse Carbon Microspheres on a Large Scale. The Journal of Physical Chemistry C. 2009; 113(19): 8455–8459. doi: 10.1021/jp811356a
35. Sevilla M, Fuertes AB. The production of carbon materials by hydrothermal carbonization of cellulose. Carbon. 2009; 47(9): 2281–2289. doi: 10.1016/j.carbon.2009.04.026
36. Liu X, Zhang Z, Guo W. van der Waals screening by graphenelike monolayers. Physical Review B. 2018; 97(24). doi: 10.1103/physrevb.97.241411
37. Zhang M, Yang H, Liu Y, et al. Hydrophobic precipitation of carbonaceous spheres from fructose by a hydrothermal process. Carbon. 2012; 50(6): 2155–2161. doi: 10.1016/j.carbon.2012.01.024
38. Szeluga U, Kumanek B, Trzebicka B. Synergy in hybrid polymer/nanocarbon composites. A review. Composites Part A: Applied Science and Manufacturing. 2015; 73: 204–231. doi: 10.1016/j.compositesa.2015.02.021
39. Lin Y, Xu H, Gao Y, et al. Preparation and characterization of hydrochar-derived activated carbon from glucose by hydrothermal carbonization. Biomass Conversion and Biorefinery. 2021; 13(5): 3785–3796. doi: 10.1007/s13399-021-01407-y
40. Wei P, Li Z, Zhang Y, et al. Structure and properties of aromatic naphthalene thermotropic liquid crystal copolyester/MWCNT composites. International Journal of Polymer Analysis and Characterization. 2023; 28(4): 293–306. doi: 10.1080/1023666x.2023.2211727
41. Biswas B, Balla P, Krishna BB, et al. Physiochemical characteristics of bio-char derived from pyrolysis of rice straw under different temperatures. Biomass Conversion and Biorefinery. 2022; 14(12): 12775–12783. doi: 10.1007/s13399-022-03261-y
42. Chaves Fernandes BC, Ferreira Mendes K, Dias Júnior AF, et al. Impact of Pyrolysis Temperature on the Properties of Eucalyptus Wood-Derived Biochar. Materials. 2020; 13(24): 5841. doi: 10.3390/ma13245841
43. Huang R, Liu X, Qi F, et al. Efficient preparation of carbon nanospheres-anchored porous carbon materials and the investigation on pretreatment methods. Bioresource Technology. 2022; 344: 126235. doi: 10.1016/j.biortech.2021.126235
44. Kong X, Zhu Y, Lei H, et al. Synthesis of graphene-like carbon from biomass pyrolysis and its applications. Chemical Engineering Journal. 2020; 399: 125808. doi: 10.1016/j.cej.2020.125808
45. Zhou H, Zhan Y, Guo F, et al. Synthesis of biomass-derived carbon aerogel/MnO composite as electrode material for high-performance supercapacitors. Electrochimica Acta. 2021; 390: 138817. doi: 10.1016/j.electacta.2021.138817
46. Dong S, Tang W, Hu P, et al. Achieving Excellent Electromagnetic Wave Absorption Capabilities by Construction of MnO Nanorods on Porous Carbon Composites Derived from Natural Wood via a Simple Route. ACS Sustainable Chemistry & Engineering. 2019; 7(13): 11795–11805. doi: 10.1021/acssuschemeng.9b02100
47. Ji C, Liu Y, Xu J, et al. Enhanced microwave absorption properties of biomass-derived carbon decorated with transition metal alloy at improved graphitization degree. Journal of Alloys and Compounds. 2022; 890: 161834. doi: 10.1016/j.jallcom.2021.161834

48. Srihata W, Jamnongkan T, Rattanasak U, et al. Enhanced electrostatic dissipative properties of chitosan/gelatin composite films filled with reduced graphene oxide. Journal of Materials Science: Materials in Electronics. 2016; 28(1): 999–1010. doi: 10.1007/s10854-016-5620-0
49. Zhang X, Liu J, Wang Y, et al. Effect of polyamide 6 on the morphology and electrical conductivity of carbon black-filled polypropylene composites. Royal Society Open Science. 2017; 4(12): 170769. doi: 10.1098/rsos.170769
50. Wang Q, Meng Q, Wang T, et al. High-performance antistatic ethylene-vinyl acetate copolymer/high-density polyethylene composites with graphene nanoplatelets coated by polyaniline. Journal of Applied Polymer Science. 2017; 134(37). doi: 10.1002/app.45303
51. Zhang Q, Wang J, Guo BH, et al. Electrical conductivity of carbon nanotube-filled miscible poly(phenylene oxide)/polystyrene blends prepared by melt compounding. Composites Part B: Engineering. 2019; 176: 107213. doi: 10.1016/j.compositesb.2019.107213
52. Li S, Huang A, Chen YJ, et al. Highly filled biochar/ultra-high molecular weight polyethylene/linear low density polyethylene composites for high-performance electromagnetic interference shielding. Composites Part B: Engineering. 2018; 153: 277–284. doi: 10.1016/j.compositesb.2018.07.049
53. Li S, Li X, Deng Q, et al. Three kinds of charcoal powder reinforced ultra-high molecular weight polyethylene composites with excellent mechanical and electrical properties. Materials & Design. 2015; 85: 54–59. doi: 10.1016/j.matdes.2015.06.163
54. Erickson KL. Thermal decomposition mechanisms common to polyurethane, epoxy, poly(diallyl phthalate), polycarbonate and poly(phenylene sulfide). Journal of Thermal Analysis and Calorimetry. 2007; 89(2): 427–440. doi: 10.1007/s10973-006-8218-6
55. Balou S, Ahmed I, Priye A. From Waste to Filament: Development of Biomass-Derived Activated Carbon-Reinforced PETG Composites for Sustainable 3D Printing. ACS Sustainable Chemistry & Engineering. 2023; 11(34): 12667–12676. doi: 10.1021/acssuschemeng.3c02685
56. Ma CM, Huang Y, Kuan H, et al. Preparation and electromagnetic interference shielding characteristics of novel carbon-nanotube/siloxane/poly-(urea urethane) nanocomposites. Journal of Polymer Science Part B: Polymer Physics. 2004; 43(4): 345–358. doi: 10.1002/polb.20330
57. Kim YJ, Shin TS, Choi HD, et al. Electrical conductivity of chemically modified multiwalled carbon nanotube/epoxy composites. Carbon. 2005; 43(1): 23–30. doi: 10.1016/j.carbon.2004.08.015